Kinetic study of CO2 hydrate formation based on heat transfer measurement

Véronique Osswald, Pascal Clain, Didier Dalmazzone, Anthony Delahaye,
Laurence Fournaison

Kinetic study of CO₂ hydrate formation based on heat transfer measurement

Véronique OSSWALD[(a)], Pascal CLAIN[(a,b)], Didier DALMAZZONE[(c)], Anthony DELAHAYE[(a)], Laurence FOURNAISON[(a)]

[(a)] Université Paris-Saclay, INRAE
Antony, 92761, France, veronique.osswald@inrae.fr
[(b)] Léonard de Vinci Pôle Universitaire, Research Center
Paris la Défense, 92916, France
[(c)] ENSTA-Paris
Palaiseau 91120, France

ABSTRACT

Carbon dioxyde hydrates are ice-like crystalline solids composed of CO_2 molecules trapped inside cages of hydrogen-bonded water molecules. CO_2 hydrates slurries can be used as phase change material for industrial issues of cold distribution, due to high dissociation enthalpy of CO_2 hydrate (around 374 kJ kg⁻¹, higher than that of ice – 333 kJ kg⁻¹). However, formation rate of CO_2 hydrate is a real limitation, and the way to control and promote it is a key parameter.

The present work investigates kinetics studies of CO_2 hydrate crystallization for various pressure and stirring rate conditions in a stirred batch jacketed reactor. A heat transfer measurement method is used to determine the rate of hydrate formation. In a first time, the method has been validated by evaluating ice crystallization then it was applied to CO_2 hydrates crystallization. Finally, an empirical model have been tested for describing the experimental results and compare to other kinetics determination.

Keywords: Secondary Refrigeration, Carbon Dioxide, Hydrates.

1. INTRODUCTION

Secondary refrigeration (as illustrated by Fig. 1) consists to use an environmental friendly fluid for cold distribution and storage in order to confine primary refrigerants, reduce their quantities and thus their direct greenhouse effect due to gas emissions.
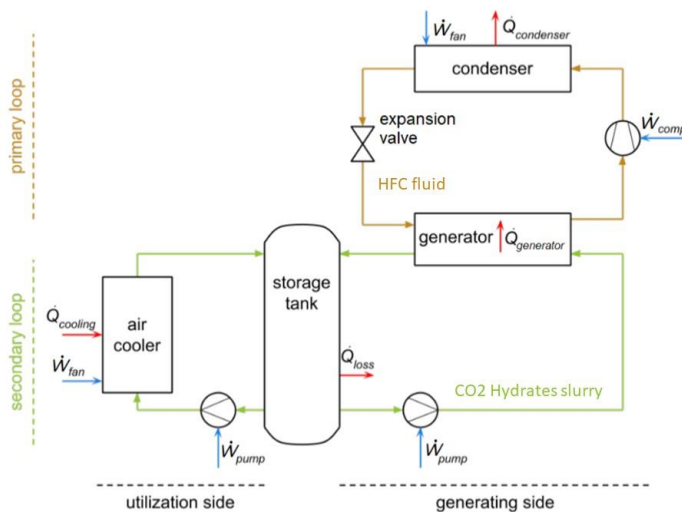

Figure 1: Secondary refrigeration system

CO_2 hydrates slurry is a promising PCM slurry for secondary refrigeration due to the high latent heat (around 374 kJ.kg^{-1}) and can be used in a wide range of temperature conditions that are suitable for air conditioning application. Clathrate hydrates of CO_2 are ice-like crystalline solids composed of CO_2 molecules trapped inside cages of hydrogen-bonded water molecules. While the thermodynamic properties of CO_2 hydrates are now well established, knowledge of crystallization kinetics phenomena is always a challenge (Warrier, P. *et al.* 2016). Trying to understand and control gas hydrate formation is a key factor since discovery of hydrates in pipeline plugs by Hammerschmidt (Hammerschmidt, E.G. 1934). Most of hydrate-based reactors at laboratory scale are equipped with pressure and temperature recorders, and many kinetic models (Englezos, P. *et al.* 1987, Englezos, P. *et al.* 1987, Skovborg, P. and Rasmussen, P. 1994) are mass balance based with assumptions on CO_2 concentration in liquid phase and on CO_2 and water molar composition of hydrates. Another method used Differential Thermal Analysis (DTA)(Clain, P. *et al.* 2015) to determine the formation rate of CO_2 and TBPB hydrate slurries. The aim of this study is to apply heat balance to the determination of CO_2 hydrate formation kinetics in a lab scale reactor.

2. MATERIAL AND METHOD

2.1. Raw material specifications

Carbon dioxide gas cylinder of 99.995% (by volume) purity purchased from Linde Gas and ultra-pure water type I, obtained from Milli-Q® water purification system, were used for experiments.

2.2. Equipment
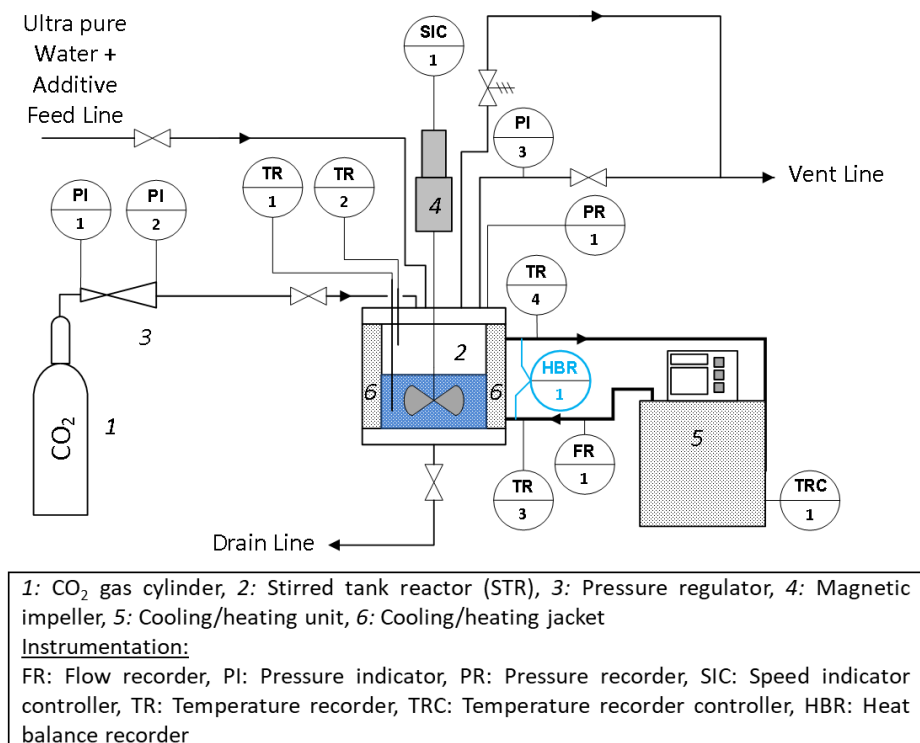
The setup used for those experiments illustrated in Fig. 2.

1: CO_2 gas cylinder, 2: Stirred tank reactor (STR), 3: Pressure regulator, 4: Magnetic impeller, 5: Cooling/heating unit, 6: Cooling/heating jacket
Instrumentation:
FR: Flow recorder, PI: Pressure indicator, PR: Pressure recorder, SIC: Speed indicator controller, TR: Temperature recorder, TRC: Temperature recorder controller, HBR: Heat balance recorder

Figure 2: Scheme of the experimental setup

The device is composed of four parts: CO_2 feed, an external refrigerating unit, a magnetic drive coupling motor agitator and a customized stainless steel reactor. The maximum operating pressure of this reactor was 3.8 MPa, with an internal volume of $1.4*10^{-3}$ m^3. The reactor was built with a cooling jacket in order to control reactor temperature set-point using a coolant (water + monopropylen glycol). The external cooling/heating unit was a Julabo FP50-HE circulator of 8L capacity, with an acceptable temperature stability of 0.01 °C. Agitator

assembly consisted of motor, variable frequency motor speed regulator, magnetic drive coupling, suitable drive mounting, shaft and 3-blades propeller. The vessel was equipped with a pressure transmitter supplied by Keller, calibrated at the laboratory and had an uncertainty of 0.1 % within the range of 0 - 4 MPa. An analogue pressure gauge (PI3) was also used to monitor pressure especially during depressurization step. The CO_2 injection pressure was controlled by a cylinder pressure regulator supplied by Messer with an outlet pressure range of 0 - 10 MPa. All the temperatures were measured by copper-constantan T type thermocouples, calibrated at the laboratory and had an uncertainty of -/+ 0.2 K. within the range of 263.15 - 298.15 K. The flow of coolant inside the cooling jacket is measured by a Rosemount 8750W magnetic flowmeter supplied by Emerson Process within a range of 0 – 40 L/hr. A special sensor has been developed to measure directly heat balance on cooling jacket. Temperature, pressure, flow and heat balance recorders are connected to a Data Acquisition system supplied by Agilent and connected to a PC. The monitoring and recording of all process values (temperatures, pressure, flow, heat balance, every 10 s) the control of CO_2 injection and temperature set-point of the heating/cooling unit were done thanks to a VBA code.

2.3. Experimental protocol

An amount of 0.7 kg of solution used for experiment was weighed in order to have a gas/liquid volume ratio inside the reactor of 1:1. The liquid solution was transferred to the reactor and then the air was removed with a vacuum pump. Thanks to a model based on a CO_2 mass balance and previously developed by Marinhas cf. Eq. (1) (Marinhas, S. *et al.* 2006) , the initial mole number of CO_2 , $n_{CO2,tot}$, was set to obtain a final hydrates fraction value estimated of 25 wt%. This model assuming that the dissolution equilibrium is reached at each moment and set the value of nb_h at 7.23.

$$n_h = \frac{n_{CO_2,tot} - \sigma_{CO_2}\dfrac{\rho_{H_2O}V_l}{M_{H_2O}} - \left(\dfrac{P_{CO_2}}{Z(P_{CO_2},T)TR}\right)\left(V_{tot} - (n_{H_2O,l} - nb_h)(M_{H_2O} + \sigma_{CO_2}M_{CO_2})\right)}{1 - \sigma_{CO_2}nb_h + \left(\dfrac{P_{CO_2}}{Z(P_{CO_2},T)TR}\right)\left(nb_h(M_{H_2O} + \sigma_{CO_2}M_{CO_2}) - \dfrac{M_h}{\rho_h}\right)} \qquad \text{Eq. (1)}$$

The speed set-point of the stirrer was fixed at 850 rpm, which is a mid-high-value within a range of 400 and 1200 rpm. Then the reactor was fed with CO_2. A part of this CO_2 was solubilized in water. Initial pressures corresponding to this CO_2 hydrates fraction was 3.28 MPa for an initial temperature of 291.15K.
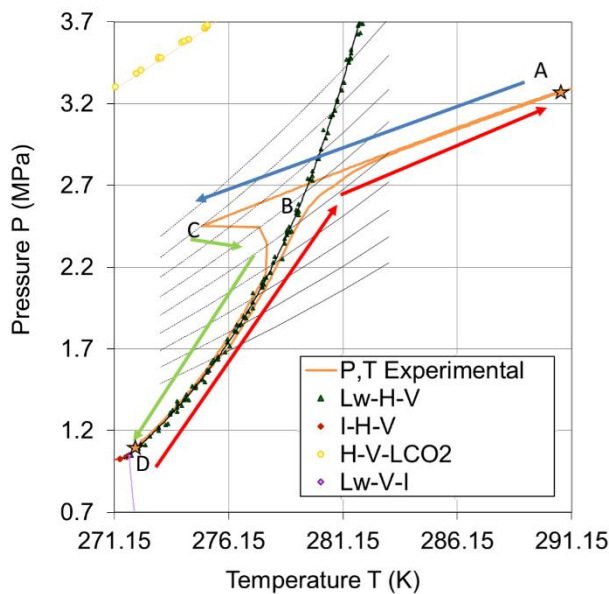

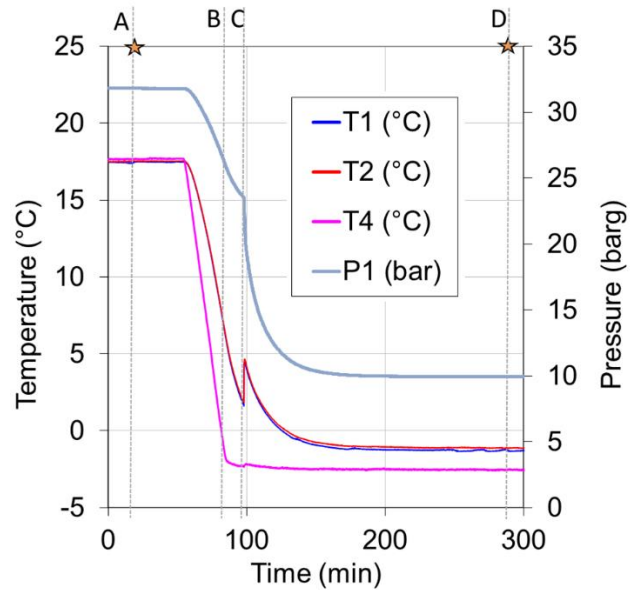
Figure 3: Pressure-Temperature diagram

Figure 4: Pressure and temperature evolution during time

When the equilibrium value of solubility for the initial pressure and temperature was reached (see point A), a cooling protocol was applied for the reactor contents. The ending value of the cooling/heating unit temperature and the cooling rate in -0.7 K/min were set and controlled. After crystallization occurred (see point C), CO_2 hydrates formation was achieved when pressure stabilized with no further drop (see point D on Fig. 3 and Fig. 4).
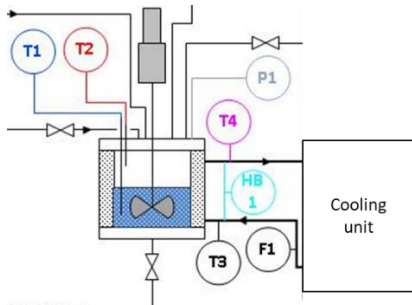
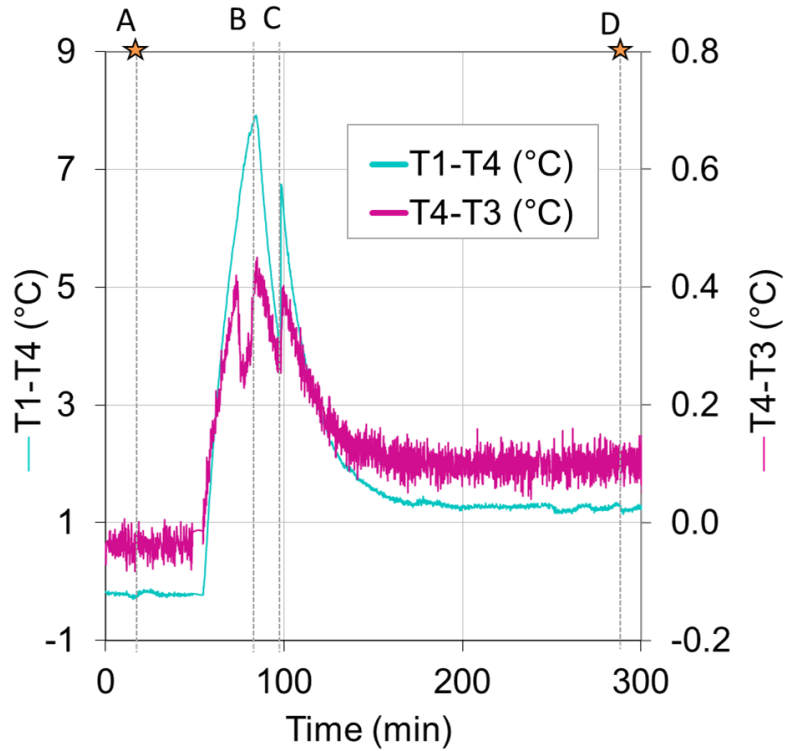## 3. EXPERIMENTAL RESULTS AND DISCUSSION

Figure 5: Reactor sensors

Figure 6: Temperature differences (T1-T4) and (T4-T3) vs. time

Fig. 5 shows the sensors placed on the reactor. There is two thermocouples inside the reactor, one for the liquid phase (T1), the other one for the gas phase (T2) and there is two other thermocouples at the inlet (T3) and the outlet (T4) of the cooling jacket. There is two way to determine heat transfer between reactor and cooling jacket. On one hand the temperature difference between T inside reactor (T1) and T cooling jacket (T4) to calculate heat flow between reactor and cooling jacket; and on the other hand the difference between T outlet cooling jacket (T4) and T inlet cooling jacket (T3) to calculate heat balance on the cooling jacket thanks to flow rate F1. The power obtained from the difference T1-T4 requires the determination of the global exchange coefficient U and the exchange surface area A (see Eq. (2)). The power obtained from the temperature difference T4-T3 requires the measurement of the flow rate F through the cooling jacket.

$$HB_{T1-T4} = U * A * (T_1 - T_4)$$

Eq. (2)

$$HB_{T4-T3} = F_1 * \rho * c_P * (T_4 - T_3)$$

Eq. (3)

Fig. 6 shows the temperature difference T1-T4 and the temperature difference T4-T3 during the hydrate crystallization shown in Fig. 4. The temperature difference between the reactor and the cooling jacket is significant, both during the liquid cooling phase (maximum 8 °C) and during the hydrate crystallization (6.7 °C). Nevertheless, the overall exchange coefficient U and the exchange area A cannot be determined directly from experiments, as these parameters change during hydrate formation. The temperature difference between the outlet and the inlet of the cooling jacket, T4-T3, is very small between - 0.1°C and + 0.4°C and the signal is very noisy (see Fig. 6). The order of magnitude of this temperature difference was the same as the measurement uncertainty. A direct measurement of the heat balance was developed to solve this problem (see Eq. (4)).

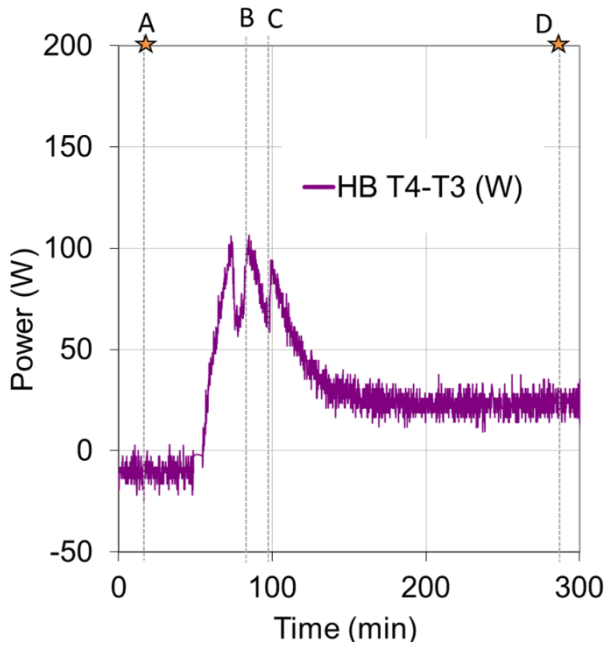$$HB_1 = F_1 * \rho * c_P * \Delta T_1 \qquad \text{Eq. (4)}$$
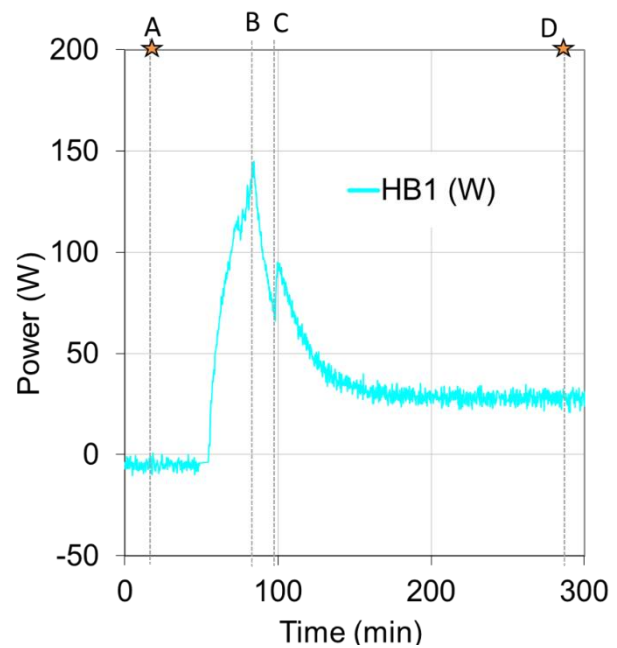

Figure 7: Heat balance T4-T3 vs. time

Figure 8: Heat balance with direct measurement vs. time

Fig. 7 and Fig. 8 show respectively the power obtained in Watt with temperature difference T4-T3 and with direct measurement during the same run as described previously (see Fig. 4). The HB1 signal is less noisy than the HB T4-T3 signal. The standard deviation between these two measurements is divided by 5 for stabilized temperature conditions during the calibration. In order to determine the fraction of hydrates crystallized, this power signal integrated for each time step (t2-t1) and the amount of hydrates obtained between these two instants calculated from Eq. (5). Hydrate fraction at time t2 was cumulative sum of all the hydrate quantities obtained from the beginning of the crystallization until t2.

$$\Delta x_{HYD} = \frac{\left[((1 - x_{HYD}(t_1)) * Cp_{H_2O} + x_{HYD}(t_1) * Cp_{HYD}) * (T_1(t_2) - T_1(t_1)) + \frac{HB_1 * \Delta t}{m_{H_2O,ini}} \right]}{\Delta H_{HYD}^{formation} + \frac{1}{2}(Cp_{H_2O} - Cp_{HYD}) * (T_1(t_2) - T_1(t_1))} \qquad \text{Eq. (5)}$$

Fig. 9 shows a comparison of the evolution of mass hydrate fraction versus time with regards to a material balance (blue curve) or a heat balance (red curve). Hydrate formation is achieved at t = 200 min, i.e. around

100 minutes after the supercooling break. Table 1. shows characteristics times of hydrate formation in order to obtain 50 % and 90 % of the final hydrate mass fraction.

Table 1: Characteristics times of hydrate crystallization

	$t_{0.5}$ (min)	$t_{0.9}$ (min)
Mass balance	3	26.8
Heat balance	10.1	33.7

The rate of crystallization indicated by the mass balance is faster than the one given by the heat balance. It may be due to the assumptions used to calculate the amount of hydrates crystallized at each time, such as the concentration of CO_2 dissolved in the liquid phase equal to the solubility of CO_2 in the liquid for the experimental conditions of temperature and pressure or the filling rate of the cages. Final hydrate fraction calculated based on the mass balance was 23.5 % as compared to 24.8 % for the one obtained from the heat balance, corresponding to a difference of 5.3 %. This difference can be linked to the fact that the whole heat transfer from the double-shell to the reactor is not used only for the crystallization of the hydrates and the cooling of the liquid+solid phase, and therefore the quantity of hydrates formed is overestimated.
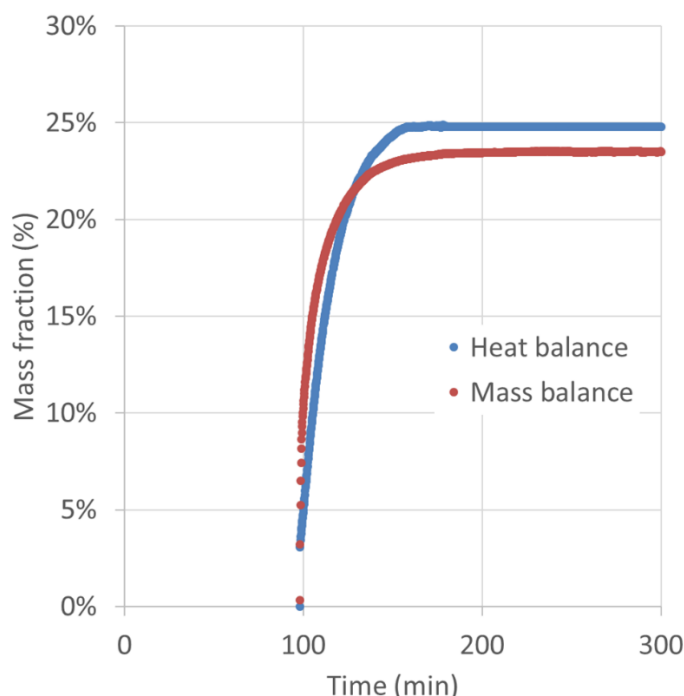

Figure 9: Hydrates mass fraction vs. time based on mass balance (red curve) and on heat balance (blue curve)

4. CONCLUSIONS

Thanks to a dedicated experimental device, the monitoring of CO_2 hydrate formation during crystallization was done classically by mass balance, but also by heat balance. Slight differences observed between these two methods can be explained by the assumptions made to calculate the mass balance and by the fact that there may be some heat losses, which are not taken into account in the empirical mass balance model developed. Others experiments under different operating conditions have to be run in order to validate this promising method. Moreover, these measurements coupled with, for example, in-situ and real time particle size analysis will improve the determination of the crystallization kinetics of CO_2 hydrates.

ACKNOWLEDGEMENTS

NOMENCLATURE

P	pressure (Pa)	R	universal gas constant, $R = 8.314$ ($J \times mol^{-1} \times K^{-1}$)
T	temperature (K)	V	volume (m^3)
M	molecular mass ($kg \times mol^{-1}$)	Z	gas compressibility (dimensionless)
n	number of moles, mol	nb_h	hydrate number ($mol_{H2O} \times mol_{CO2}^{-1}$)
x	hydrate mass fraction (%)	ΔH	molar latent heat of dissociation ($J \times mol^{-1}$)
C_p	specific heat capacity ($J \times kg^{-1} \times K^{-1}$)	PW	power (W)
H-V	Hydrate-Vapor	*L-H*	Liquid-Hydrate
L-H-V	Liquid-Hydrate-Vapor	*L-V*	Liquid-Vapor

Subscripts

g	Gas	*h*	Hydrate
i	Initial	ℓ	Liquid
mol	Mole	*vol*	Volume
w	Water		

Greek letters

ρ	density, $kg \times m^{-3}$	σ	solubility, $mol \times mol^{-1}$

REFERENCES

Warrier, P., Khan, M. N., Srivastava, V., Maupin, C. M. and Koh, C. A., 2016. Overview: Nucleation of clathrate hydrates. J. Chem. Phys., 145(21).

Hammerschmidt, E. G., 1934. Formation of Gas Hydrates in Natural Gas Transmission Lines. Ind. Eng. Chem., 26(8), 851-855.

Englezos, P., Kalogerakis, N., Dholabhai, P. D. and Bishnoi, P. R., 1987. Kinetics of formation of methane and ethane gas hydrates. Chem. Eng. Sci., 42(11), 2647-2658.

Englezos, P., Kalogerakis, N., Dholabhai, P. D. and Bishnoi, P. R., 1987. Kinetics of gas hydrate formation from mixtures of methane and ethane. Chem. Eng. Sci., 42(11), 2659-2666.

Skovborg, P. and Rasmussen, P., 1994. A mass transport limited model for the growth of methane and ethane gas hydrates. Chem. Eng. Sci., 49(8), 1131.

Clain, P., Osswald, V., Spiga, O., Delahaye, A. and Fournaison, L., 2015. A new formation kinetic study method of TBPB and CO2 hydrates based on DTA. ICR2015 : The 24th IIR International Congress of Refrigeration, Yokohama, Japan.

Marinhas, S., Delahaye, A., Fournaison, L., Dalmazzone, D., Fürst, W. and Petitet, J.-P., 2006. Modelling of the available latent heat of a CO_2 hydrate slurry in an experimental loop applied to secondary refrigeration. Chemical Engineering and Processing, 45(3), 184-192.